05

Second harmonic microscopy from nearsurface plasma ignited by tightly focused femtosecond fiber laser beam

© A.A. Garmatina[1], E.I. Mareev[1], A.A. Korshunov[1,2], M.D. Mozhaeva[1,2], N.V. Minaev[1], A.E. Muslimov[1], D.N. Khmelenin[1], V.E. Asadchikov[1], V.M. Gordienko[1,3]

[1] Kurchatov Complex of Crystallography and Photonics NRC „Kurchatov Institute“, 123182 Moscow, Russia
[2] National Research Nuclear University ”MEPhI”, 115409 Moscow, Russia
[3] Moscow State University, Department of Physics, 119992 Moscow, Russia

e-mail: e-mail: alga009@mail.ru

Received December 11, 2023
Revised January 09, 2024
Accepted January 16, 2024

Method measuring in real time the size of the microplasma, which is a source of X-rays, ignited on the target surface by a tightly focused ($NA = 0.2$) repetition rate femtosecond fiber laser beam (280 fs, $10-25\,\mu$J) has been developed. The technique based on the backreflected second harmonic signal from the microplasma. It has been stated that the size of the microplasma second harmonic beam is $\sim 8.5\,\mu$m at the pulse energy of $10\,\mu$J, pulse repetition rate of 2 MHz, which corresponds to the regime of achieving the maximum X-ray yield and minimum of the microplasma size. The conversion efficiency at laser intensity of $\sim 10^{14}$ W/cm^2 into the second harmonic is about 10^{-6}.

Keywords: fiber laser, femtosecond laser pulse, backreflected laser plasma second harmonic.

DOI: 10.61011/EOS.2024.01.58287.11-24

Introduction

Currently, powerful optical fiber lasers generating picosecond and femtosecond pulses are widely used in fundamental and applied research [1,2]. Compared with solid-state lasers, fiber lasers are distinguished not only by good beam quality ($M^2 \sim 1$), high mean power (tens of watts) as well as long-term stable operation that is particularly important for applications such as laser-plasma micromachining. Commercially available femtosecond lasers characterized by low single pulse energy ($10-50\,\mu$J), but due to high pulse repetition rate ($0.1-10$ MHz), high mean power is achieved to ensure high process performance.

Laser-plasma micromachining of a material is followed by an ablation phenomenon — emission of laser-induced target material particles existing within the time interval up to several hundred nanoseconds. When intensity is about 10 TW/cm^2 and higher, micromachining may be followed by X-ray generation [3]. X-ray generation, on the one hand, may indicate efficient energy coupling into hot surface plasma. On the other hand, when vacuum intensities are about 1 PW/cm^2 and higher, X-ray radiation is of individual interest for creation of X-ray sources as an alternative to traditional X-ray tubes [4].

The next generation of femtosecond lasers with high repetition rate conditions is also distinguished by changing paradigm in micro laser-plasma processing of materials and accompanying processes such as X-ray generation. This enhance the interest in the use of this phenomenon for creation of radiographic research devices that are alternative to standard microfocus sources [5]. However, tight focusing ($NA > 0.1$) shall be used in a low-energy femtosecond optical fiber laser circuit (energy per pulse$\sim 1-40\,\mu$J) in order to achieve intensities required to generate X-ray radiation and create a minimum-size X-ray source.

In most cases, the target micromachining mode is used in standard atmosphere conditions and is followed not only by the ablation process, but also by a set of spurious accompanying phenomena [6]. Ionization of ambient atmosphere (usually air) resulting in absorption of the laser energy and also in beam profile distortion caused by the self-defocusing process is also one of significant limiting factors associated with laser emission energy delivery to the target [7]. Though the influence of ionization depends on such factors as the ambient atmosphere composition, wavelength, pressure and focal volume, general plasma formation threshold for pico-femtosecond near-infrared pulses in air is $\sim 2 \cdot 10^{13}$ W/cm^2. It should be noted that for pulses of about $100-200$ fs, effective energy loss under tight focusing ($NA \sim 0.2$ and higher) and vacuum intensity of about $10-100$ TW/cm^2 is negligent due to small focal volume [7], however, defocusing can result in considerable increase in the beam diameter (by more than a factor of 1.5) resulting in limited effective intensity.

Significant effects in the process of micromachining with femtosecond laser pulses, following at a high repetition rate, include the screening of laser energy by ablated particles.

They are located in the near-surface region and not having time to settle by the time of the arrival of the next laser pulse. Enother proses ismay be absorption of energy in residual ablation plasma. An important difference from the effect of atmospheric ionization in this case is the lifetime and density of the ablation cloud of particles, which ensures the absorption of subsequent pulses on a time scale of up to several microseconds.

The literature also observes the effect of heat accumulation, which influences the prosess of laser matter interaction [6,9]. The femtosecond laser ablation of metals is also reported to be followed by the clusterized substance release and aggregation processes in the plasma plume [10].

All factors listed above indicate that it is necessary to provide real-time monitoring of the induced microplasma spot parameters in repetition rate laser-plasma interaction ultrashort pulses and a matter. This refers both to tightly focused femtosecond laser beam setting (aiming) on the target surface and to monitoring of the produced microplasma size which is the source of X-ray photons.

This problem may be effectively solved by using second harmonic generation (SHG) simultaniously generated with X-ray photons in the laser-induced microplasma [11]. In this regard, SHG may serve as a tool for monitoring the microplasma spot size and, thus, the X-ray source size. In the normal incidence geometry of the femtosecond laser beam on the target surface, plane-wave approximation SHG is prohibited. However, the presence of longitudinal electric field component for tightly focused beams enables the back-reflected second harmonic signal to be generated [12]. In addition, laser-induced local field on a rough laser-modified target surface as a result of ablation can cause effective SHG due to resonant excitation of surface plasmon polariton modes that may exist in femtosecond-laser-induced plasma [13]. It should be noted that we have earlier recorded a second harmonic during laser-plasma micromachining of a metal target with a femtosecond laser beam with intensity 10^{16} W/cm^2 [14]. Thus, such research experience shows that the X-ray radiation and second harmonic signal are interrelated [14–16] and defined by the hot plasma parameters.

The research focuses on the development of a method for online monitoring of microplasma (being the source of X-ray photons and second harmonic) size induced by femtosecond optical fiber laser on the target surface. The method is based the optical microscopy of the back-reflected laser-induced second harmonic spot generated in the surface plasma exposed to tightly focused femtosecond optical fiber laser beam in high pulse repetition rate conditions.

Experimental setup

The experiments were performed using a femtosecond ytterbium fiber laser ANTAUS-10W-40u/250K. The laser emitted radiation at a wavelength of 1030 nm with maximum pulse energy of 40 mkJ, pulse duration 280 fs, an average power up to 20 W. Single pulse energy was calculated using the repetition rate and average power. During the experiment, the laser pulse repetition rate varied up to 2 MHz, $M^2 = 1.2$, beam diameter was 4 mm. The concept and details of the experimental setup are described in [17].

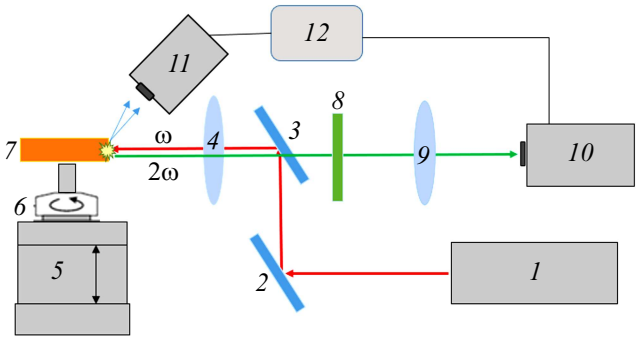

Figure 1. Experimental setup *1* — femtosecond optical fiber laser; *2, 3* — mirrors; *4* — focusing lens $NA \sim 0.2$; *5* — linear translator; *6* — motor; *7* — copper target; *8* — optical filters; *9* — focusing lens; *10* — CCD camera/fiber-optic spectrometer; *11* — X-ray detector; *12* — personal computer.

Laser emission was focused normally on the side surface of the cylindrical copper target 44 mm in diameter and 8 mm in height by PAL-20-NIR-HR-LC00 lens with a focal distance of $f = 10$ mm (numerical aperture $NA = 0.2$). The target was attached to the motor axle and installed on a five-axis motor-operated slide. A special algorithm ensured vertical cyclic movement of the rotating target at a constant speed. Rotation speed was equal to 5000 rpm, vertical movement speed was 50 mm/min.

Microcraters occurred on the target surface after one vertical pass of the acting tightly focused laser beam as a result of ablation. So, surface became uniformly modified within about 10 s. The target material microprocessing rate was about 9 μm in 5 min.

To prevent sputtering of ablated particles onto the focusing optics, compressed air blowing into the exposure area was used. Experimental unit scheme is presented in Fig. 1.

Focus position relative to the target was controlled by the X-ray radiation measured using SCSD-4 single-channel scintillation detector.

To get the second harmonic spot images, a microscope was fabricated that included a short-focus lens with a focal distance of $f = 6$ cm and transferred the magnified plasma and second harmonic images to the CCD matrix of XCAM1080PHA digital camera in order to measure the hot plasma area. Optical system has achieved a spatial resolution of 0.3 μm/pixel. For simultaneous recording of optical spectra and beam image, a beam-splitting plate could be installed in the optical path of the CCD camera to divert a part of emission that was further focused by the lens with a focal distance of $f = 5$ cm to the optical fiber inlet. Plasma and second harmonic spectra were recorded using USB4000 spectrometer.

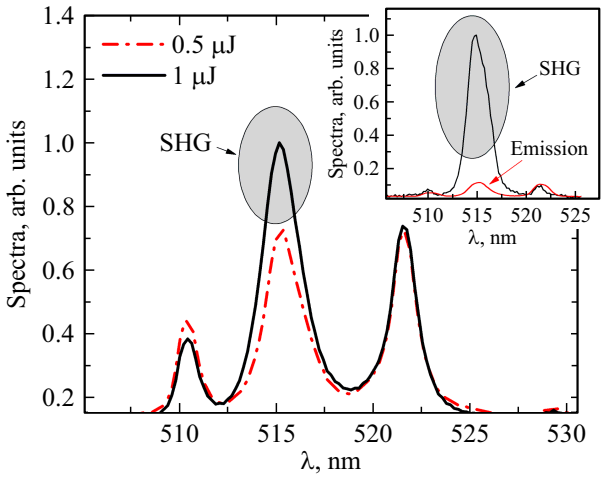

Figure 2. Copper emission spectrum at 0.5 μJ (red) and second harmonic spectrum against the emission spectrum at 1 μJ (black). The detail shows the emission spectrum at 0.5 μJ (red) and second harmonic spectrum together with the emission spectrum at 10 μJ (black), frequency is 2 MHz. Spectra were normalized to 521 nm line amplitude everywhere. The second harmonic (SHG) is shown by grey ovals.

Results

During formation of laser microplasma on the copper target surface exposed to the femtosecond fiber laser with varying laser parameters (repetition rate, energy per pulse), maximum X-ray photon yield $N \sim 1.6 \cdot 10^9$ ph/s in 2π sr was achieved at a laser pulse repetition rate of 2 MHz [17]. In this mode, the maximum single pulse energy was equal to 10 μJ at a mean power of 20 W. Thus, this mode was of the most interest for us in terms of the beam size measurement.

To develop the hot plasma area control procedure in terms of the second harmonics, spectral measurements of the back-reflected spectrum were carried out in order to detect whether the second harmonic spectrum is present in it. Since the laser-induced emission spectrum of copper „covers“ the second harmonic emission spectrum of the fiber laser, then it was important to find whether the second harmonic signal can be extracted from the plasma background in experiment conditions. For this, the second harmonic and plasma spectra were measured depending on the energy and repetition rate. It has been found that emission spectrum at a laser pulse repetition rate of 2 MHz was recorded at 0.5 μJ. It should be noted that amplitudes of 521 and 515 nm lines occur to be comparable at this intensity. The second harmonic falls on 515 nm line and coincides with the copper emission line, therefore its presence in the spectrum was identified by a distinctive increase in 515 nm line amplitude over 521 nm line. When the energy rises to 1 μJ (meets the vacuum intensity up to $I \sim 3 \cdot 10^{13}$ W/cm^2), 515 nm spectral line signal amplitude occurs to be higher than 510 and 521 nm emission line amplitude which is indicative of the initial stage of second harmonic extraction from the emission background (Figure 2).

For ease of comparison, the curves on the figure were normalized to 521 nm line amplitude. With further increase in the energy, the increase in 515 line amplitude over the emission spectrum is growing, and at the maximum energy of 10 μJ, the second harmonic contrast against emission achieves ~ 10 (see the detail in Figure 2) demonstrating the stable extraction of the second harmonics over the plasma background. The second harmonic is shown by grey ovals in Figure 2. It should be noted that when the second harmonic signal is outside the emission line, the signal-to-noise ratio shall increase significantly. As for the reference point, the second harmonic emission of the main laser emission generated using a standard nonlinear optical converter was used for this.

In order to fulfil the set out task, we measured the time dependences of X-ray yield and second harmonic signal amplitude (in the spectrum maximum) that demonstrate the correlation. An example of such dependence at single pulse energy of 10 μJ and repetition rate of 2 MHz is shown in Figure 3, *a*. Behaviors of the X-ray yield and second harmonic signal amplitude have much in common when varying the laser energy (and, respectively, the vacuum intensity) (Figure 3, *b*).

Thus, using previous literature data on signal correlation [11,16] as well as the obtained data, we believe that the size of hot plasma responsible for the second harmonic signal is close to the size of plasma responsible for X-ray generation. Therefore the estimated second harmonic spot size may be used to assess the X-ray source size.

It is apparent that the experimentally obtained points for the second harmonic signal are approximated by the exponential function with exponent $Y_{2w} \sim I^{2.3}$, at the same time, the X-ray photon yield is approximated by $Y \sim I^3$. Both signals demonstrate nonlinear growth when energy increases up to 6 μJ, which is satisfied by the corresponding intensity $\sim 1.5 \cdot 10^{14}$ W/cm^2. For clarity, dependence $Y \sim I^{2.8}$ averaged for two curves is shown in Figure 3, *b*. It should be noted that a close exponent of 2.6 was observed in [18], where the SHG process was studied at an inclined (45°) exposure to a microjoule-level single femtosecond laser pulse on the aluminum target in the vacuum chamber. However, in our experiments with further growth of the single pulse energy (more than 6 μJ), the dependence shows that saturation condition occurs. In this condition, experimental points are below the approximation curve both for X-ray radiation and second harmonic. We believe that such dependence behavior and the presence of saturation are associated with the features of high repetition rate interaction between the femtosecond fiber laser emission and the target.

Since the ablation rate also grows with increasing pulse energy, this means that the weight of the ablated material increases. In addition, according to [8], the recombination time of plasma in the surface area achieves microsecond units. Thus, increase in the single tightly focused femtosecond laser pulse energy (and vacuum intensity, respectively) initiates the increase in electron concentration in the created

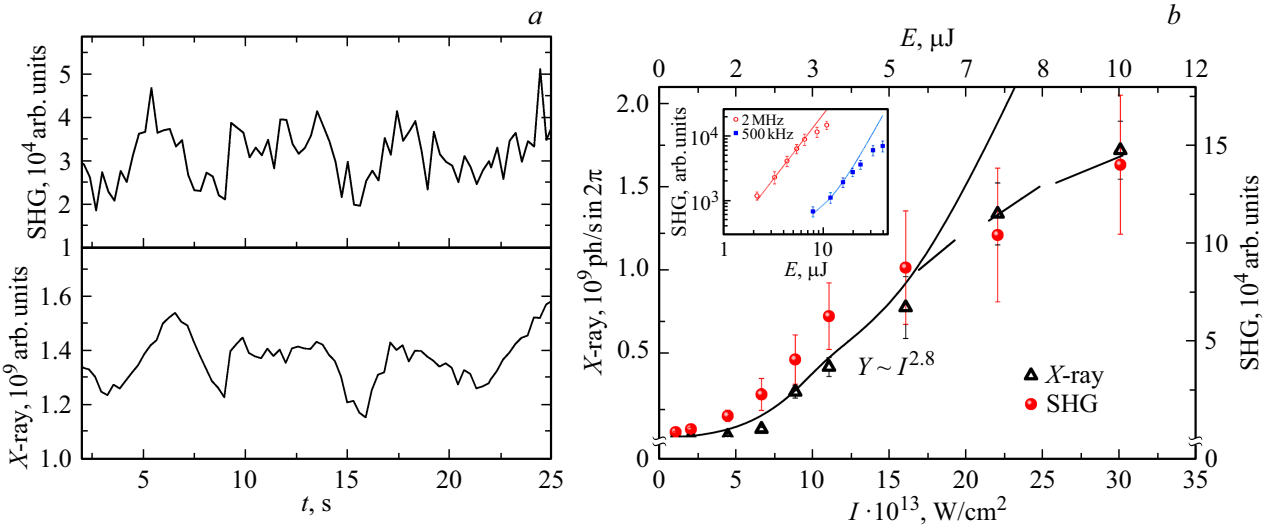

Figure 3. Temporal dynamics of the second harmonic signal (amplitude in the spectrum) (upper) and integral X-ray signal (lower) at energy 10 μJ and repetition rate 2 MHz (*a*). Dependence of the X-ray signal (black, triangles) and second harmonic signal amplitude (red, circles) on the vacuum intensity and femtosecond pulse energy at a repetition rate of 2 MHz. The detail shows the dependence of the second harmonic signal on the single pulse energy at 2 MHz (red) and 500 kHz (blue) (*b*).

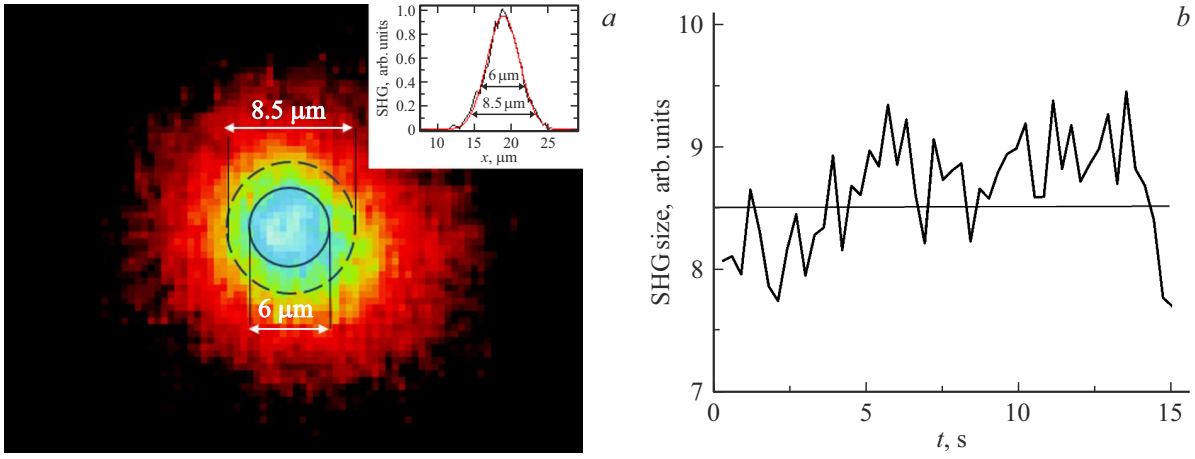

Figure 4. Second harmonic beam image on the CCD camera at 10 μJ and repetition rate 2 MHz. The detail shows the second harmonic beam profile (*a*). Temporal dynamics of the second harmonic beam diameter taken by level $1/e^2$ at pulse energy10 μJ and generation frequency 2 MHz (*b*).

two-component medium (mixture of air and ablated copper microparticles). This results from the ambient ionization process with simultaneous demonstration of clamping effect [7,19] due to accompanying ionization self-defocusing of the laser beam. Whilst the target surface in the interpulse time interval is in a substantially heated condition that additionally complicates the interaction picture [6,9].

The performed experiments show (see the detail in Figure 4) that at a laser pulse repetition rate of 500 kHz saturation occurs at high single pulse energy $\sim 20\,\mu$J. This is indicative of the influence of repetition rate variation on the ionization process and, respectively, on the electron concentration. It should be noted that the second harmonic signal selection against the emission spectrum background at this repetition rate took place also at a higher laser energy (2 μJ, vacuum intensity about $6 \cdot 10^{13}$ W/cm^2), and as specified above this value is 4 times higher than at a pulse repetition rate of 2 MHz.

The second harmonic signal depends on the laser emission intensity like the X-ray signal. There is a correlation between the X-ray signal and second harmonic signal. As specified in [17], dependence of the X-ray radiation signal on the femtosecond laser pulse repetition rate is a highly nonlinear process. Such dependence on repetition rate at fixed energy was also obtained for the second harmonic (not shown here). We believe that the intensity of laser beam interacting with the target grows with laser pulse repetition rate at fixed energy per pulse. This, in our opinion, occurs due to emerging gas-dynamic conditions in the target surface area (see the text below). This also

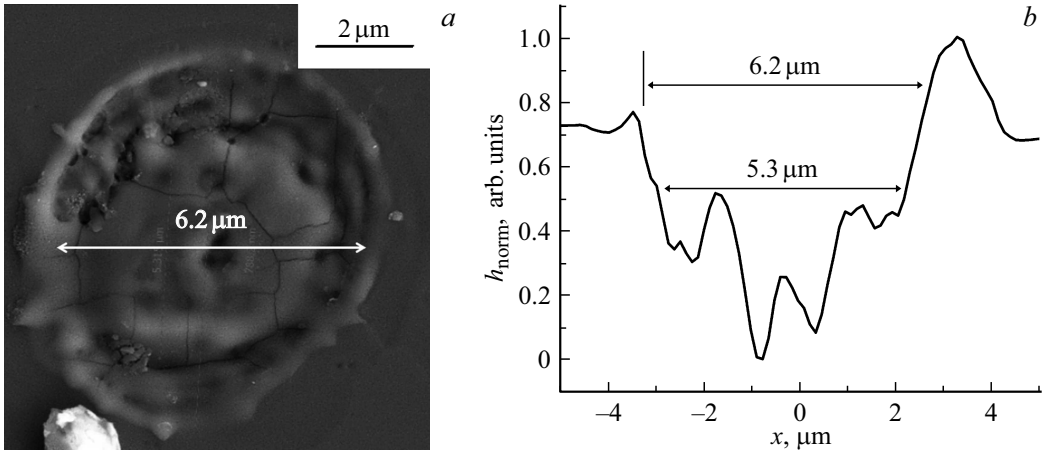

Figure 5. Electronic microscopy of a sapphire surface modification at a single laser pulse energy of $9\,\mu$J, vacuum intensity $\sim 3 \cdot 10^{14}$ W/cm^2 (a); crater profile on the sapphire plate surface according to the atomic-force microscopy data, single laser pulse energy $9\,\mu$J (b).

results in decrease in the second harmonic signal extraction energy threshold with increasing laser pulse repetition rate. Spectral data recording time variation did not influence the relation of amplitudes of 521 nm copper emission line and 515 nm line on which the second harmonic emission was „superimposed".

In addition, as shown in [18], ratio of conversion into the second conversion for the electron plasma is about 10^{-20} cm^2/W. The measured second harmonic signal power is $20\,\mu$W, thus, the conversion efficiency is about 10^{-6}. It should be noted that this conversion efficiency may serve for assessment of the laser intensity on the target. Due to ionization and defocusing, real intensity brought to the target will differ from the vacuum intensity and will not be directly measurable. Knowing the conversion efficiency and its correlation to the intensity, real laser intensity on the target may be estimated as about 10^{14} W/cm^2.

After recording the presence of the second harmonic that is extracted from the emission spectrum with high contrast, we proceeded to the second harmonic microscopy in order to define its size for characterization of the laser-plasma source of X-ray radiation. We measured the plasma spot using its magnified imaging setup. To assess the size of back-reflected second harmonic, we recorded the beam image on the CCD camera. The obtained data were used to restore its profiles that were approximated by the Gaussian function. The software calculated the beam size by level $1/e^2$ and displayed the data. Beam sizes in pixels were displayed every 0.3 s synchronously with the X-ray signal and second harmonic amplitude. Then averaging was performed within the time period of about 15 s. Then, the target was removed after the measurements and replaced with a measuring scale with a known scale interval of $50\,\mu$m, whose image was used to calculate magnification on the camera. The magnification in this setup was about 8. Then beam size in pixels was converted into microns.

The back-reflected second harmonic beam from the laser-induced microplasma was recorded within a repetition rate range of 0.8–2 MHz and at a mean power of 20 W that corresponded to an energy range of $8-25\,\mu$J. Figure 4, a shows the second harmonic beam image recorded by the CCD camera for 2 MHz. Size dynamics at level $1/e^2$ during 15 s is shown in Figure 4, b. As shown in Figure 4, a, the most intense hot plasma region (core, white-blue) is about $6\,\mu$m, this corresponds to the beam size at level $1/e$. Then, this is followed by a lower intensity region containing the second harmonic shown in yellow and corresponding to the beam size at level $1/e^2$. Its size is about $8.5\,\mu$m. The last boundary zone corresponds to the plasma image and is shown in red. The image size limited by the dynamic range of the camera is about $15\,\mu$m. Since the plasma percentage in the spectrum is about 10%, then the beam size at level $1/e^2$, in our opinion, reflects the second harmonic beam size.

Critical point in the research was the assessment of the induced ionization nonlinearity effect of the ambient air on the laser beam parameters that should occur in interaction between a single tightly focused pulse and target surface [20]. For this, the copper target in the experiment was replaced with polished flat sapphire crystal placed perpendicularly to the laser emission propagation direction. Sapphire ablation threshold is ~ 9 J/cm^2 or $\sim 6 \cdot 10^{13}$ W/cm^2 at a pulse width of about 150 fs [21] that is close, in our case, to the initial recording stage of the X-ray radiation and second harmonic. Therefore the crater size may be used to describe the hot plasma region size responsible for the investigated processes, and then this size may be compared with the spot size of the second harmonic induced in the plasma in order to verify the offered technique and assess the effect of the ablated particle cloud on the beam size.

To form single-exposure craters, the laser pulse repetition rate (50 Hz) was set in such a way as to provide sufficient stepping motor speed for target movement into a fresh region before each new exposure. Using the prepared target offset algorithm, craters were obtained with different focus

position relative to the crystal surface at various energies. Then the craters were analyzed using electron and atomic-force microscopes. Craters at laser focus on the surface were chosen by the following criterium: minimum diameter and maximum depth.

We had studied the influence of the induced ionization nonlinearity of the ambient air depending on the energy in within $9-30\,\mu$J (vacuum intensity of the laser beam $3\cdot10^{14}-9\cdot10^{14}\,$W/cm^2, vacuum diameter of the focused beam $3.9\,\mu$m), that can be exhibited as defocusing that occurs during interaction between the single tightly focused laser beam and target surface. Crater image and profile obtained using the electron and atomic-force microscopes a laser pulse energy of $9\,\mu$J are shown in Figure 5. If the crater profile is approximated by the Gaussian function, then a typical size may be identified in it at level $1/e^2$ and is equal to $\sim 6.2\,\mu$m, and a size may identified at level $1/e$ and is about $5.3\,\mu$m. For comparison with the second harmonic spot diameter, level $1/e^2$ was assumed.

It should be noted that the crater profile recorded using the atomic-force microscope is similar to the pattern analyzed in [22] in comparable conditions of tightly focused femtosecond laser beam effect on a dielectric target.

The data in Figure 6 show that the crater size demonstrates almost a linear growth beginning from the energy about $9\,\mu$J ($I_{\text{vac}}\sim 3\cdot10^{14}\,$W/cm^2) up to $30\,\mu$J ($I_{\text{vac}}\sim 9\cdot10^{14}\,$W/cm^2). Such behavior corresponds to the demonstration of the ionization self-defocusing effect resulting from the clamping effect [7] due to which it is stabilized at a particular level and further energy increase results only in beam diameter growth. It should be noted that defocusing is manifested as early as at $9\,\mu$J resulting in the increase in the crater size ($\sim 6.2\,\mu$m) compared with the vacuum beam size ($\sim 4\,\mu$m) by a factor of 1.5.

The reference measurements of the crater diameter formed in the sapphire (in air) exposed to the tightly focused single femtosecond pulse make it possible to assess the ionization effect now in a two-component (ablated particle cloud in air) medium on the second harmonic beam size when the copper target was exposed to the repetitively-pulsed fiber laser emission. By comparing the crater sizes and second harmonic spot diameter at comparable energy (the second harmonic sizes were measured not only at different energies, but also at $0.8-2\,$MHz of the generated laser pulses) (Figure 6), we obtain that, despite large measurement errors, the mean crater sizes are lower than the laser-plasma spot size of the second harmonic by about a factor of 1.5. Thus, for $10\,\mu$J, the second harmonic size is $8.5\,\mu$m, and the crater size is — $6.2\,\mu$m. Such discrepancy is probably due to the additional ionization self-defocusing effect in a two-component medium (air containing ablated particles) above the target surface on the second harmonic spot diameter. The second harmonic diameter measurements throughout the energy range demonstrate a typical trend towards increasing plasma spot and second harmonic spot diameters due to the effect detected by us.

As for the plasma spot size measurements using the second harmonic signal, the plasma spot diameter „stabilization“ mode is probably associated with the features of

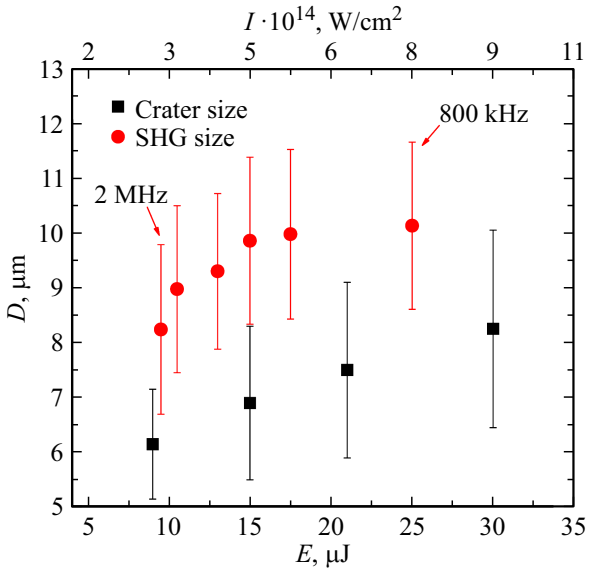

Figure 6. Dependence of the laser-plasma diameter of the second harmonic diameter beam (red, ovals) and crater (black, boxes) formed on the sapphire crystal plate surface at various laser pulse energies and mean powers 20 W.

interaction between the repetition rate femtosecond laser emission (having a high single-pulse energy density) and the target in the ambient gas when a complex gas-dynamic pattern occurs in the target surface region. Theoretical model of such process occurring when the target is exposed to tightly focused ($0.5-1\,$MHz) intense femtosecond laser pulses has not been developed yet. However, some features of high repetition rate (up to 100 kHz) pulsed (nanosecond) laser exposure (energy density of tens J/cm^2) of the target in the ablation mode are known [23]. In this case, a relatively long-living vacuum region (low gas concentration at high temperature) is formed in the target surface area. Parameters of this region naturally depend on the energy density and generation pulse repetition rate. Whilst the surface medium vacuum decreases the plasma shielding effect and defocusing due to decreasing amount of plasma forming substance, and the temperature rise in the surface area reduces the probability of ablated particle aggregation, thus, affecting the ionization conditions. As a result, quasi-equilibrium plasma forming conditions and, therefore, stabilization of the second harmonic plasma spot may occur. We will continue the efforts to create the process model.

Conclusion

We have developed a real-time size monitoring technique for the microplasma formed on the target surface by a tightly focused ($NA=0.2$) repetitively-pulsed (repetition rate $0.8-2\,$MHz) femtosecond (280 fs) optical fiber laser beam with a single pulse energy within $10-25\,\mu$J using the second harmonic signal back-reflected from the microplasma. It has been found that nonlinearity of the laser-induced two-component medium (ablated particles in air)

influences the self-consistent SHG process (accompanied by the X-ray photon yield) occurring when the copper target surface is exposed to tightly focused repetition rate femtosecond fiber laser in plasma forming regime. It has been also found that the second harmonic laser-plasma beam size and, thus, the microplasma spot size (responsible for X-ray photon generation) at $10\,\mu$J and vacuum intensity $3 \cdot 10^{14}$ W/cm^2 of a single pulse in the sequence of pulses generated by the optical fiber laser is equal to $8.5 \pm 1.6\,\mu$m. efficiency of laser emission conversion into the second harmonic was about 10^{-6}, which corresponds to the actual laser intensity on the target $\sim 10^{14}$ W/cm^2.

The research findings open an opportunity of using the developed technique for online monitoring not only of a microfocus laser-plasma X-ray source size by the back-reflected second harmonic signal, but also of accurate focusing to a target surface, microchanneling, film perforation using laser-plasma ablation micromachining of materials by next generation femtosecond fiber lasers operating at high pulse repetition rate.

Acknowledgments

The authors are grateful to I.G. Dyachkova, Yu.M Dymshits and V.V. Koldaev for their assistance in experiments.

Funding

The research has been carried out under the state job-order of Research and Engineering Center „Kurchatov Institute“ in terms of optical research and under agreement with the Ministry of Education and Science № 075-15-2021-1362 in terms of creation of a microfocus source.

Conflict of interest

The authors declare that they have no conflict of interest.

References

[1] T. Wang, C. Li, B. Ren et al. High Power Laser Science and Engineering, **11**, e25 (2023). DOI: 10.1017/hpl.2023.12
[2] A. Tünnermann, C. Momma, S. Nolte. Appl. Phys. A, **129**, 157 (2023). DOI: 10.1007/s00339-023-06403-9
[3] J. Thøgersen, A. Borowiec, H. Haugen, F. McNeill, I. Stronach. Appl. Phys. A, **73**, 361–363 (2001). DOI: 10.1007/s003390100741
[4] L. Martín, J. Benlliure, D. Cortina-Gil, A. Haruna, C. Ruiz. Physica Medica, **82**, 163–170 (2021). DOI: 10.1016/j.ejmp.2020.12.023
[5] A.A. Garmatina, V.E. Asadchikov, A.V. Buzmakov, I.G. Dyachkova, etc. Crystallografiya, **67** (6), 1012 (2022) (in Russian). DOI: 10.1134/S1063774522060074
[6] D. Brinkmeier, D. Holder, A. Loescher, Ch. Röcker et al. Appl. Phys. A, **128**, 35 (2022). DOI: 10.1007/s00339-021-05156-7
[7] V.A. Aleshkevich, V.M. Gordienko, B.G. Bravy. JOSA B, **40** (5), 1031–1038 (2023). DOI: 10.1364/JOSAB.484265
[8] K. Pangovski, O. Otanocha, Sh. Zhong, M. Sparkes at al. Appl. Phys. A, **123**, 114 (2017). DOI: 10.1007/s00339-016-0589-3
[9] J. Finger, M. Reininghaus. Optics Express, **22** (15), 18790n (2014). DOI: 10.1364/OE.22.018790
[10] M. Oujja, J. Izquierdo, L. Bañares, R. de Nalda, M. Castillejo. Chem. Phys., **20**, 16956 (2018). DOI: 10.1039/C8CP02825G
[11] A.B. Savelev, S.A. Akhmanov, I.M. Bayanov, S.V. Gaponov et al. Proc. SPIE, **1627**, 334 (1992). DOI: 10.1117/12.60175
[12] N.I. Koroteev, V.A. Makarov, S.N. Volkov. Optics Commun., **138**, 113–117 (1997). DOI: 10.1016/S0030-4018(97)00032-1
[13] V.M. Gordienko, S.A. Magnitsky, T.Yu. Moskalev, V.T. Platonenko. Izvestiya RAN. Ser. fizicheskaya, (in Russian). **60** (3), 10–17 (1996).
[14] V.M. Gordienko, I.A. Zhvaniya, A.S. Khomenko. SPIE Proceed., **7994**, 79940P (2011). DOI: 10.1117/12.881882
[15] L. Gizzi, D. Giulietti, A. Guiletti, P. Audebert, S. Bastiani, J. Geindre, A. Myayrowicz. Phis. Rev. Lett., **76** (13), 2278 (1996). DOI: 10.1103/PhysRevLett.76.2278
[16] V.M. Gordienko, I.A. Makarov, E.V. Rakov. Proc. SPIE, **6606**, 66060S (2007). DOI: 10.1117/12.729640
[17] A.A. Garmatina et al. Optics Express, **31** (26), 44259–44272. (2023). DOI: 10.1364/OE.502200
[18] D. von der Linde, H. Schulz, T. Engers, H. Schiiler. IEEE J. QE, **28** (10), 2388 (1992) DOI: 10.1109/3.159545
[19] A.A. Garmatina., B.G. Bravy, F.V. Potemkin, M.M. Nazarov, V.M. Gordienko. J. Phys. Conf. Ser., **1692**, 012004 (2020). DOI: 10.1088/1742-6596/1692/1/012004
[20] R. Yamada, W. Komatsubara, H. Sakurai, K. Konishi et al. Optics Express, **31** (5), 7363–7382 (2023). DOI: 10.1364/OE.482986
[21] L. Qi, K. Nishii, M. Yasui, H. Aoki, Y. Namba. Optics and Lasers in Engineering, **48** (10), 1000–1007 (2010). DOI: 10.1016/j.optlaseng.2010.05.006
[22] S. Kudryzshov, P. Danilov, A. Rupasov, S. Khonina et al. Optical Materials Express, **10** (12), 3291 (2020). DOI: 10.1364/OME.412399
[23] S.M. Klimentov, P.A. Pivovarov, V.I. Konov, D. Braitling, F. Dausinger. Kvant. elektron., **34** (6), 537–540 (2004). (in Russian) DOI: 10.1070/QE2004v034n06ABEH002769

Translated by E.Ilinskaya